A014

Comparing Facies Realizations – Defining Metrices on Realization Space

H.H. Soleng* (Norwegian Computing Center), A.R. Syversveen (Norwegian Computing Center) & O. Kolbjørnsen (Norwegian Computing Center)

SUMMARY

A typical workflow for generating flow simulation grids goes through a facies modelling step. This typically involves setting up a stochastic model that is supposed to capture the important properties of the facies bodies in the reservoir volume in question and their uncertainties. This may be difficult or impossible within a particular modelling framework. Either we end up with a model too simple to be able to reproduce the characteristics of the reservoir, or the model parametres become too many and too difficult to specify. Hence users ask for methods able to reproduce the properties of a training image automatically. In any case one would like objective measures of similarity of facies realizations so that one is able to determine if a set of realizations have the properties that one wants.

Here we discuss possible components in a metric on a space of facies realizations and present an implementation of a facies realization analyzer program. The algorithm simply scans a number of realizations and computes the global volume fractions of each facies and the number of facies bodies of each type. Then it computes the surface areas, volumes, and extensions in each directions for the bodies and performs simple statistical analysis of the realizations and compare it with properties of a training image.

We present results of applying this software on facies realizations produced with variogram based methods, multipoint methods, and sequential Markov random fields.

The analyzer algorithm is fast, applicable in 2D and 3D, and the results are in excellent agreement with the subjective impression of similarity or dissimilarity obtained through visual inspection.

1. Introduction

Traditional variogram-based techniques have been widely used in the petroleum industry for estimation and simulation of geological and petrophysical property fields. In the general non-stationary case, difficulties in variogram model selection and parametre estimation represent a serious problem with these methods. In practice therefore, one restricts oneself to simple stationary variograms, and as a result, it is often felt that these techniques are unable to represent the complex structures observed in nature.

The *raison d'être* of multipoints methods is that they claim to give better representations of complex structures than is possible with variogram-based (two-point) methods. In addition they are very user friendly since they are able to make direct use of prior models represented by training images rather than abstract variogram models and parametres.

Any method able to generate new facies realizations based on a training image would face two challenges. The first challenge is to capture and represent all *essential* properties of the training image. The second is to produce realizations spanning a sufficient volume of realization space with the correct statistics given this representation.

In this paper we focus on the quantification of facies image properties. To this end we have implemented a body detector and analyzer program (see Algorithm 1 in Appendix A). This program is then applied to two-dimensional training images of three types and to realizations made by Snesim [1], a sequential indicator simulator, and a Markov mesh method. The results are compared with the statistics of the training image.

The Snesim algorithm and the sequential indicator simulation are well known and used by industry. Markov mesh models are not commonly seen in reservoir modelling, and thus a short presentation is given. Markov mesh models or unilateral models are well known in the statistical literature [2, 3], and is used in image processing [4]. The Markov mesh model operates by a systematic sequential simulation path running top to down and left to right in the grid. Figure 1 illustrates the situation at a fixed time in the simulation process. At this time all the cells above the current cell and all cells to the left of the current cell at the same level have already been simulated. These are indicated by filled squares in Figure 1. The cells to the right at the same level and below still remain to be simulated. These cells are indicated by stapled squares in the figure. The gray cell with the question mark is to be simulated. The probability that this cell is red is dependent only on a limited number of the previously simulated cells. These cells denote a sequential neighbourhood. An example of such a set is illustrated in Figure 1 by the cells within the solid black line. After simulation of the current cell, one steps to the right and repeats the process and so on. Boundary effects are solved by padding the simulation region. Daly [5] estimates the probabilities from the frequencies in the training image similar to what is done in Snesim. In the Markov mesh models presented in this paper the probabilities are estimated from the training image using logistic regression. Functions of the cells in the sequential neighbourhood are used as explanatory variables and the cell it self as a dependent variable.

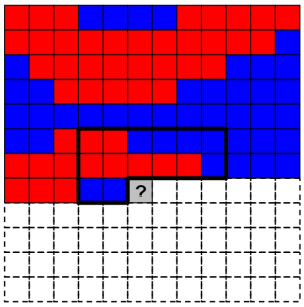

Figure 1: Sequential neighbourhood.

From the outset we like to stress that our focus is on the comparison method and not on the simulation methods. No attempt has been made to manually fine tune parametres of the simulation packages; except for the neighbourhood size we used default values. Hence, the results should *not* be regarded as test results of the simulation methods.

2. A metric in realization space

The state space of all possible facies realizations on a grid with n cells and f facies is finite with n^f possible states giving $1/2n^f(n^f+1)$ metric components. Obviously this is unmanagable.

Instead of a full-fledged realization space metric, we would like to perform a dimensional reduction to a mini-realization space metric [*]. Hence instead of pixel-wise comparison we select a few larger-scale criteria each representing an axis in mini-realization space, and represent realizations as points in this low-dimensional space.

Facies realizations could be compared along a multitude of axes defined by patterns either based on a priori or on statistical information. In this paper we suggest comparison criteria based on, in principle, observable measures such as global volume fractions (a measure of abundane), maximal directional extension of facies bodies (a measure of connectivity), and ratio of surface area to volume (a measure of ruggedness and shape). These criteria are believed to be the most important for petroleum applications. For realizations with a sufficiently large number of bodies, one could use statistics of the body measures as comparison criteria. Looking at a training image (TI), we

[*] This is analogous to the mini-superspace approximation in quantum cosmology.

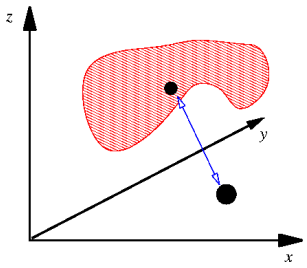

Figure 2: A metric in realization space tells us the distance between two realizations or between a training image and the sample space of a model.

could denote its position in mini-realization space as $\mathbf{X}(\mathrm{TI})$. The difference between a realization r and the training image along the axis X^i would then be

$$\Delta X^i = X^i(\mathrm{TI}) - X^i(r).$$

For a given simulation method one could then study the statistics of ΔX^i for a large number of realizations and hence also be able to say something about the distance between a training image and the sample space of a simulation method.

In principle we could write down a realization metric on the form

$$ds^2 = \sum_{i=1}^{N_{\mathrm{cr}}} \sum_{j=1}^{N_{\mathrm{cr}}} G_{ij} \Delta X^i \Delta X^j,$$

where G_{ij} a positive definite matrix (diagonal if all criteria are orthogonal), and N_{cr} the number of comparison criteria.

In order for this to make sense, one would first have to establish orthogonal criteria and second be able to establish to relative importance of each factor. Since the relative importance of the criteria probably are problem-dependent, we have not attempted to write down an explicit expression for the full metric.

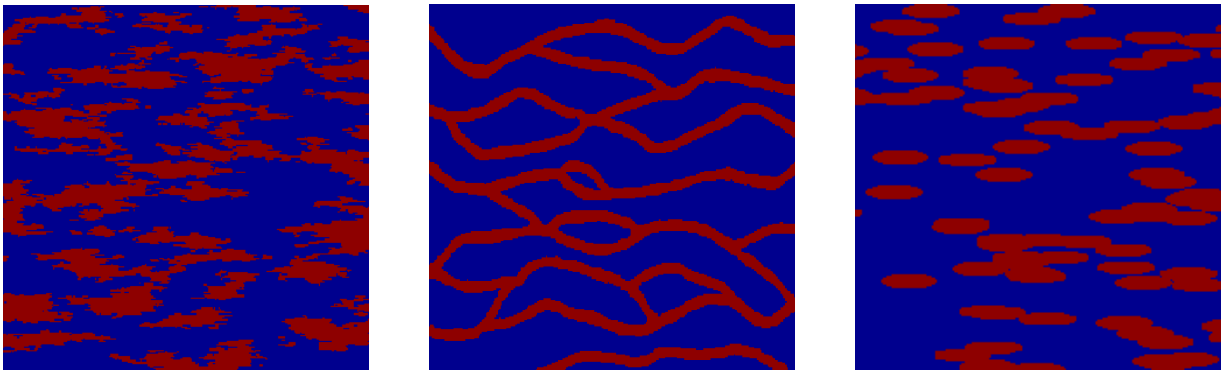

(a) Rugged (b) Channels (c) Ellipsis

Figure 3: Training images at resolution $250 \times 250 \times 1$. The x-direction is horizontal and y is vertical.

3. Tests

We appplied our method to the training images in Figure 3. Interestingly, these three training images have very similar variograms. The first training image has been generated by the sequential indicator simulation program Sisim in the open source SGeMS package [6]. To the authors, the parametres used for generating the training image were unknown. Also, we do not know how the other two training images have been created.

For each of the training images we ran the facies body analyzer to find the following comparison criteria: (i) the mean value of the area to volume ratio $\overline{A/V}$, (ii) the maximal extensions in x and y directions $\mathrm{Max}(X)$ and $\mathrm{Max}(Y)$, (iii) the mean volume $\overline{V}$, (iv) the mean area $\overline{A}$, (v) the p75 quartile for the x-extension $p75(X)$, (vi) the number of bodies n, (vii) the global volume fraction μ. For each criterium and for each training image we chose

units so that the training image value is unity for all criteria. With this normalization any set of realizations similar to the training image should then have comparison criteria values near unity.

Then, using the training images as input we generated 1000 realizations using three different methods: (i) variogram estimation and sequential indicator simulation from a commercial software package [7], (ii) multipoint statistics as implemented in Snesim from the SGeMS package [6, 1], (iii) the Markov mesh method.

3.1. Rugged body realizations

For this particular training image (3(a)) the variogram-based technique has the advantage of playing on its home ground. In order to speed up the simulations, the sequential indicator simulation software allows the user to limit the number of neighbourhood points used in the indicator kriging equations. We used 16 (the default value), 32 and 64 neighbours. Visually the results were similar to the training image in all cases even for the smallest neighbourhood size. In Figure 4 we present four random images using a neighbourhood size of 32. Increasing to 64 had no effect on the results.

In Snesim we used a template size of 30, 100, and 400 (the maximum allowed). For the rugged bodies, a template size of 100 seemed sufficient.

Judged by visual appearance all methods produced results similar to the training image, and it is not easy to say which set is most similar to it. However, according to our comparison criteria as illustrated in the whisker plots in Figure 7, the sequential indicator simulation method gave results closest to the training image. Both of the other two methods produced too many tiny objects giving too many objects in total and consequently also a too small mean volume of the objects. These methods also were too low on the p75 quartile for the maximal x extension.

For this particular case, the sequential indicator simulations was both faster and more accurate than the multipoint method in the sense that the resulting realizations were more similar to the training image. This should not come as a surprise since the training image was generated with a similar tool as the one used here.

3.2. Channel realizations

In this section we look at a training image with a fluvial-like channel structure (Figure 3(b)).

For the variogram-based technique, the channel image was impossible to reproduce[†]. Results for a neighbourhood size of 32 are shown in Figure 8.

Snesim produced channel-like objects even for relatively small template sizes, but to avoid too many dead ends we had to increase the template size to the maximal allowed value of 400. For this value the results in Figure 9 became rather similar to the training image.

The Markov mesh method produced good channels, however, with a thickness that varies too much.

From the whisker plot in Figure 11(a) the failure of the variogram-based technique is obvious. The other two methods come out with very similar results. One should perhaps come up with criteria able to detect dead ends and channel thichness variations to be able to discriminate better between the two.

3.3. Elliptic body realizations

The innocent-looking elliptic bodies (Figure 3(c)) were a challenge for two of the techniques.

Not surprisingly, the variogram-based sequential indicator simulation method failed by producing bodies which were far too rugged. This is reflected int the whisker plot in Figure 15(a) where the mean ratio of area to volume comes out far too high.

The multipoint method reproduced the features of the training image quite well; the number of bodies comes out a little high and the mean ratio of area to volume is on the high side. Increasing the template size from 100 to the maximal value of 400 only marginally improved these two properties and left the other unchanged.

The Markov mesh method ran into some problems with artifacts such as diagonal striping patterns and a somewhat too pronounced tendency for clumping. Nevertheless, all criteria falls within the uncertainty although the number of objects is on the low side and the horizontal and vertical connectivities measured by $\mathrm{Max}(X)$ and $\mathrm{Max}(Y)$ have too high centers of gravity.

4. Conclusion

We have presented simple critera based on physically measurable quantities for comparison of facies realizations. In principle, these may be used as components in a metric in realization space, provided one is able to quantify the

[†] Using adaptive local anisotropies could improve the situation, c.f. Reference [8]

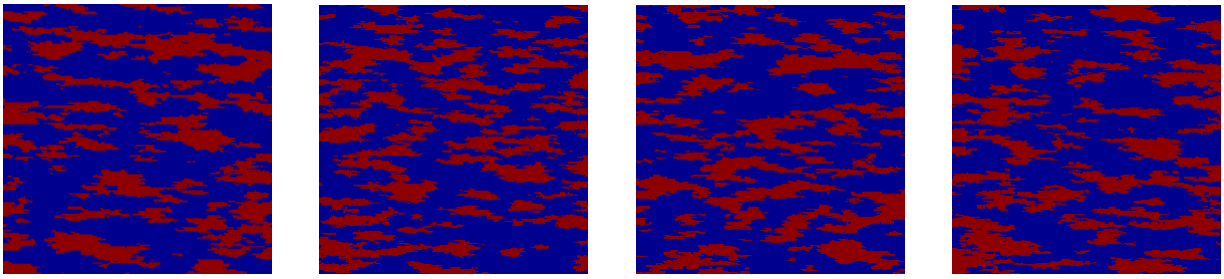

Figure 4: Four randomly choosen realizations using sequential indicator simulation with a neighbourhood size of 32.

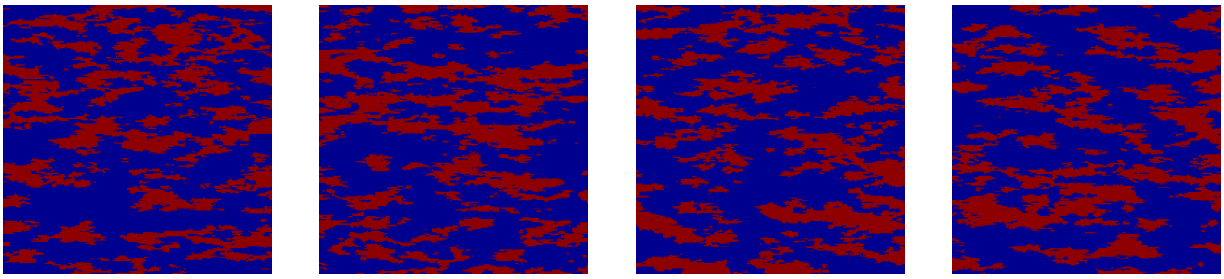

Figure 5: Four randomly choosen realizations from Snesim with template size of 100.

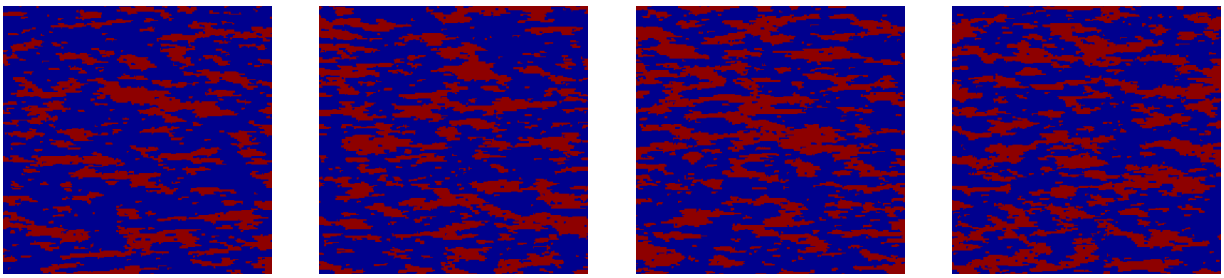

Figure 6: Four randomly choosen realizations from Markov Mesh simulations with general number of interactions.

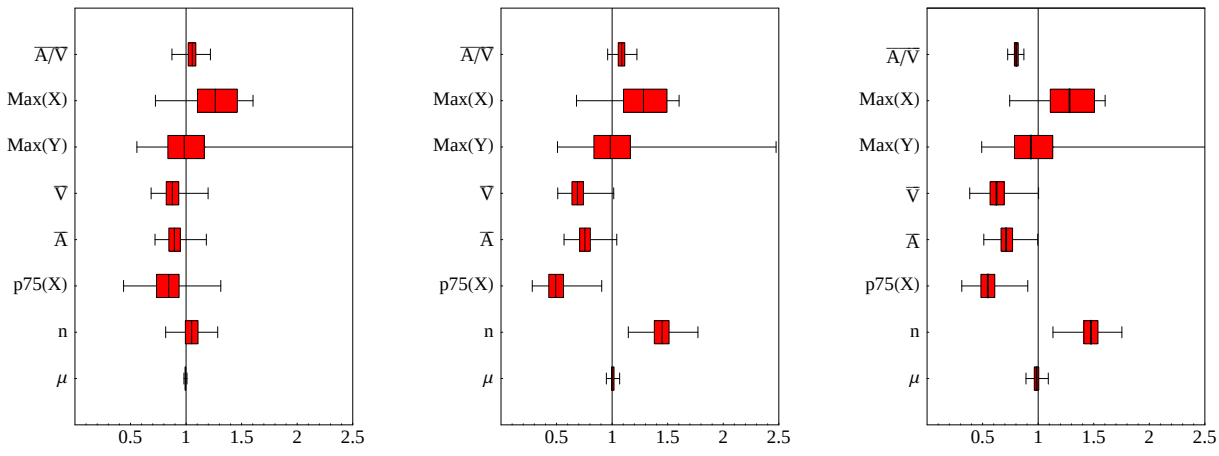

(a) Sequential indicator simulation (b) Snesim (c) Markov mesh

Figure 7: Whisker box plots for 1000 rugged body realizations from each method. The red boxes are at the 0.25 quantile. The red boxes are at the 0.25 quantile. The plots are scaled so that the value of the training image is unity. Box plots are given for mean area to volume ratio, maximal body extension in x and y directions, p75 quartile for x-extension, number of bodies, and global volume fraction.

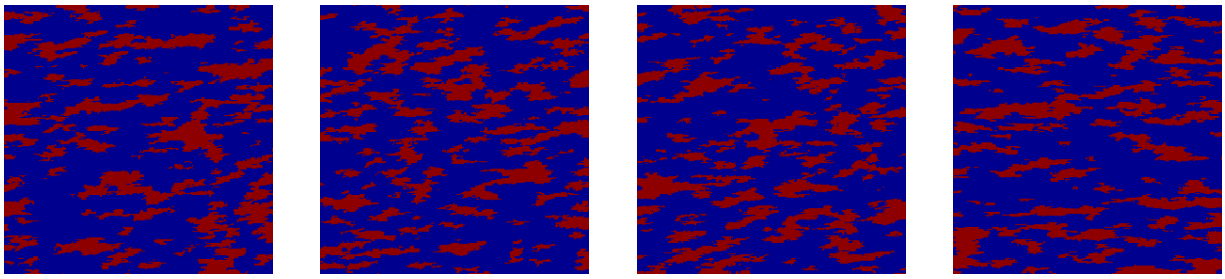

Figure 8: Four randomly choosen “channel” realizations using sequential indicator simulation with a neighbourhood size of 32.

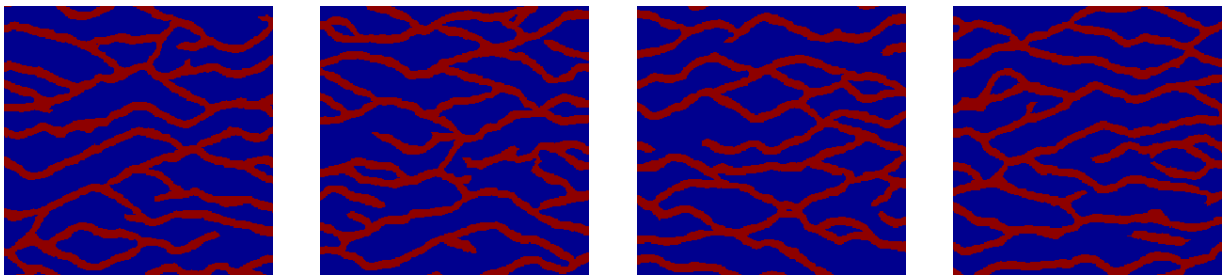

Figure 9: Four randomly choosen channel realizations from Snesim with template size of 400.

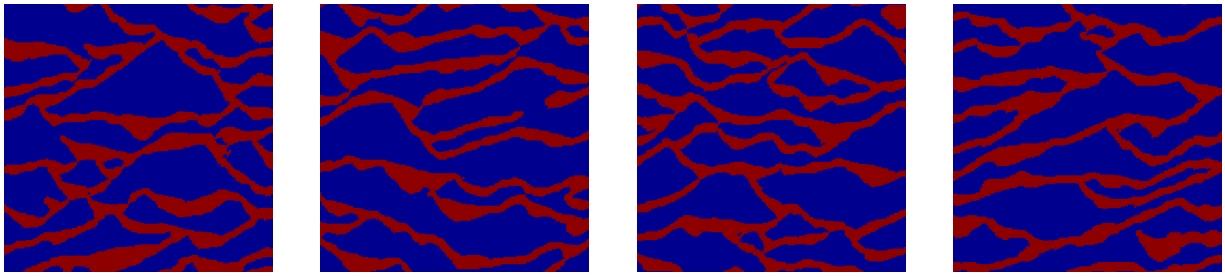

Figure 10: Four randomly choosen channel realizations from Markov mesh simulations.

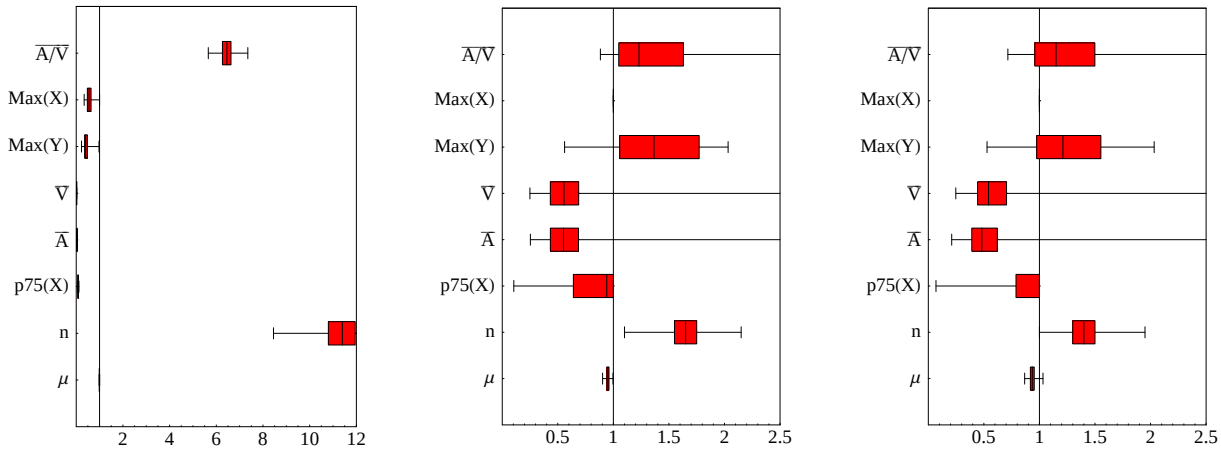

(a) Sequential indicator simulation (b) Snesim (c) Markov mesh

Figure 11: Whisker box plots for 1000 channel realizations from each method. The red boxes are at the 0.25 quantile. The red boxes are at the 0.25 quantile. The plots are scaled so that the value of the training image is unity. Box plots are given for mean area to volume ratio, maximal body extension in x and y directions, p75 quartile for x-extension, number of bodies, and global volume fraction.

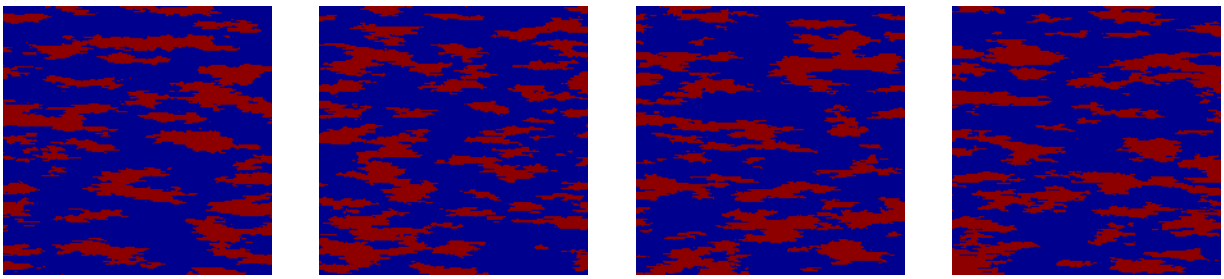

Figure 12: Four randomly choosen elliptic body realizations from sequential indicator simulation with neighbourhood size of 32.

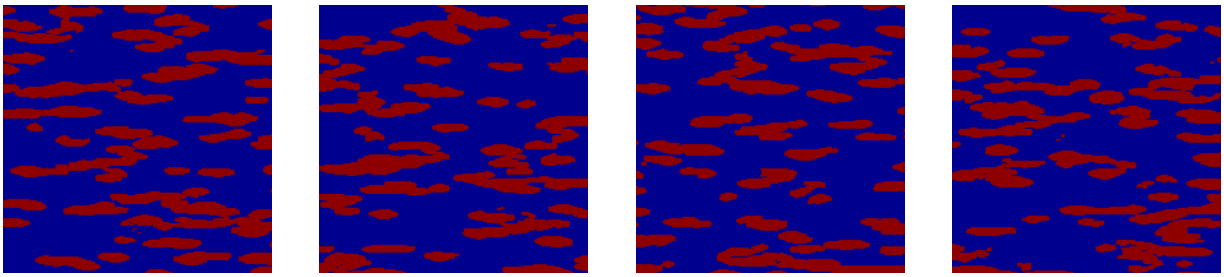

Figure 13: Four randomly choosen elliptic body realizations from Snesim with template size of 100.

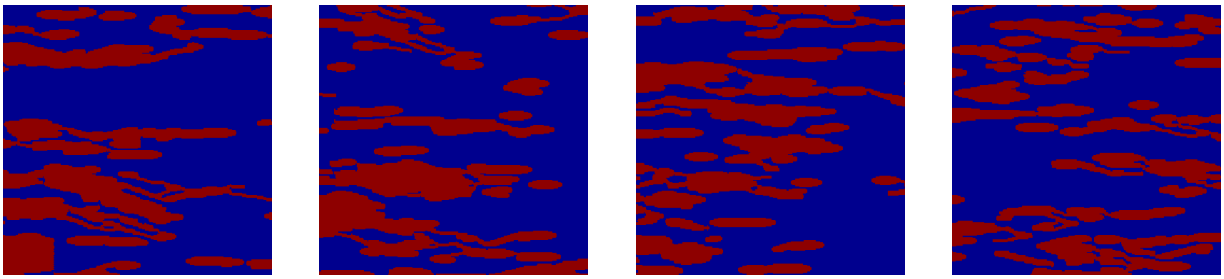

Figure 14: Four randomly choosen elliptic body realizations from the Markov mesh method.

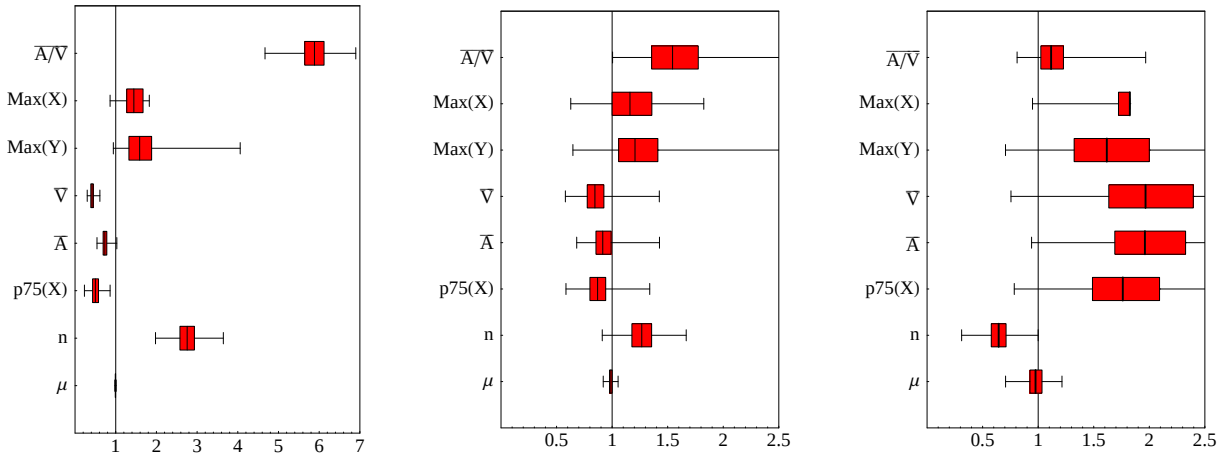

(a) Sequential indicator simulation (b) Snesim (c) Markov mesh

Figure 15: Whisker box plots for 1000 elliptic body realizations from each method. The red boxes are at the 0.25 quantile. The red boxes are at the 0.25 quantile. The plots are scaled so that the value of the training image is unity. Box plots are given for mean area to volume ratio, maximal body extension in x and y directions, p75 quartile for x-extension, number of bodies, and global volume fraction.

relative importance of each criterium and their mutual dependence.

As steps towards a metric in realization space we have tested the critera on three two-dimensional training images and three different simulation methods. While the comparison critera and the facies body analyzer algorithm both work in three dimensions, we have choosen to use two-dimensional test cases for the purpose of simple visual inspection of the results.

Test results show that the suggested critera give a good discrimination among realizations, but also that additional critera may be required to capture features such as dead end channels and variable thickness channels.

Aknowledgement

The authors would like to thank Petter Abrahamsen for comments and suggestions and Jef Caers for providing the training images. This work was supported in part by the Research Council of Norway and ENI, Hydro and Statoil under the project *Multipoint Methods for Improved Reservoir Models*.

A. Body finder algorithm

The body definition algorithm is a straightforward labelling method of order $n * N^2$ where N is the number of grid cells and n is the number of neighbours to each grid cell. It works for any number of dimensions and any grid type.

Algorithm 1 Body identification algorithm

```
1:  Assign a unique body number to each grid cell                    ▷ Initialization
2:  for each cell in grid do
3:      for each neighbour of cell do
4:          if cell belongs to same body as neighbour then
5:              new_body_number ← min(body(cell), body(neighbour))
6:              old_body_number ← max(body(cell), body(neighbour))
7:              if new_body_number < old_body_number then            ▷ Update body numbers
8:                  for each location in grid do
9:                      if body(location) equals old_body_number then
10:                         body(location) ← new_body_number
11:                     end if
12:                 end for
13:             end if
14:         end if
15:     end for
16: end for
```

References

[1] Sebastian Strebelle. *Sequential simulation drawing structures from training images*. PhD thesis, Stanford University, 2000.

[2] K. Abend, T. J. Harley, and L. N. Kanal. Classification of binary random patterns. *IEEE Trans. Inform. Theory*, 11:533–544, 1965.

[3] D. K. Pickard. Unilateral Markov fields. *Adv. Appl. Prob*, 12(3), 1980.

[4] W. Qian and D. M. Titterington. Multidimensional Markov chain models for image textures. *J. Royal Stat. Soc. B*, 53(3):661–674, 1991.

[5] Colin Daly. Higher order models using entropy, Markov random fields and sequential simulation. In Oy Leuangthong and Clayton V. Deutsch, editors, *Geostatistics Banff 2004*, volume 14/1 of *Quantitative Geology and Geostatistics*, Dordrecht, The Netherlands, 2005. Springer.

[6] The Stanford geostatistical modeling software. `http://sgems.sourceforge.net`.

[7] Irap RMS portfolio. `http://www.roxar.com`.

[8] Chris B. M. te Stroet and Judith J. J. C. Snepvangers. Mapping curvilinear structures with local anisotropy kriging. *Math. Geol.*, 37(6):635–649, August 2005.